Supplemental information for Lofton et al., Using near-term forecasts and uncertainty partitioning to improve predictions of low-frequency cyanobacterial events

Supplemental Information

Using near-term forecasts and uncertainty partitioning to improve predictions of low-frequency cyanobacterial events

Mary E. Lofton, Jennifer A. Brentrup, Whitney S. Beck, Jacob A. Zwart, Ruchi Bhattacharya, Ludmila S. Brighenti, Sarah H. Burnet, Ian M. McCullough, Bethel G. Steele, Cayelan C. Carey, Kathryn L. Cottingham, Michael C. Dietze, Holly A. Ewing, Kathleen C. Weathers, Shannon L. LaDeau

Submitted as an original research article to *Ecological Applications*

Number of pages: 39

Number of text supplements: 5

Number of tables: 7

Number of figures: 16

Number of code repositories: 1[1]

Number of datasets: 5[2]

Text S1: Data processing for potential environmental drivers of *G. echinulata* density.
Text S2: Selection of environmental covariates for Bayesian state-space models.
Text S3: Random walk model and development of informed observation error prior.
Text S4: Model ensemble exercise.
Text S5: Variability of environmental covariates in Bayesian state-space models.
Table S1: Examples of ecological forecasts with partitioned uncertainty.
Table S2: Correlation analysis for environmental covariates of *G. echinulata* density.
Table S3: Estimated mean random year effects.
Table S4: Parameter summary for all calibrated Bayesian state-space models: Part I.
Table S5: Parameter summary for all calibrated Bayesian state-space models: Part II.
Table S6: Uncertainty partitioning results across models for one-week-ahead hindcasts.
Table S7: Uncertainty partitioning results across models for four-week-ahead hindcasts.
Figure S1: Natural log-transformed *G. echinulata* colonies L^{-1} vs. growing degree days.
Figures S2-S9: Timeseries of environmental covariates used in Bayesian state-space models.
Figure S10: Timeseries of median predicted and observed *G. echinulata* density for one-week-ahead hindcasts in 2016 for the best-performing models.
Figure S11: Timeseries of median predicted and observed *G. echinulata* density for one-week-ahead hindcasts in 2015 and 2016 for models not shown in manuscript figures.
Figure S12: Timeseries of median predicted and observed *G. echinulata* density for four-week-ahead hindcasts in 2016 for the best-performing models.
Figure S13: Timeseries of median predicted and observed *G. echinulata* density for four-week-ahead hindcasts in 2015 and 2016 for models not shown in manuscript figures.
Figure S14: Uncertainty partitioning of one-week-ahead to four-week-ahead confidence intervals for 2015-2016 hindcasts for models not shown in manuscript figures.
Figure S15: Example proportional contribution of initial conditions uncertainty over time.
Figure S16: Relative contributions of process and driver uncertainty for MinWaterTempLag in 2015.

Code repository: Includes all code for data collation, model calibration, hindcasting, analysis, and visualization. Please see:

https://github.com/GLEON/Bayes_forecast_WG/tree/eco_apps_release

DOI:10.5281/zenodo.3878781

Datasets:

LSPA, K.C. Weathers, and B.G. Steele. 2020. High-Frequency Weather Data at Lake Sunapee, New Hampshire, USA, 2007-2019 ver 3. Environmental Data Initiative. https://doi.org/10.6073/pasta/698e9ffb0cdcda81ecf7188bff54445e. Accessed 2020-05-22.

Cottingham, K.L., C.C. Carey, and K.C. Weathers. 2020. Gloeotrichia echinulata density at four nearshore sites in Lake Sunapee, NH, USA from 2005-2016 ver 2. Environmental Data Initiative. https://doi.org/10.6073/pasta/b6f418436088b14666a02467797ff1ad. Accessed 2020-04-25.

LSPA, K.C. Weathers, and B.G. Steele. 2020. Lake Sunapee Instrumented Buoy: High Frequency Water Temperature and Dissolved Oxygen Data – 2007-2019 ver 1. Environmental Data Initiative. https://doi.org/10.6073/pasta/70c41711d6199ac2758764ecfcb9815e. Accessed 2020-05-16.

Cottingham, K.L., C.C. Carey, and K.C. Weathers. 2020. High-frequency temperature data from four near-shore sites, Lake Sunapee, NH, USA, 2006-2018 ver 1. Environmental Data Initiative. https://doi.org/10.6073/pasta/3e325757f0e981d91cd297f257f05f55. Accessed 2020-05-16.

Lofton, M.E., J.A. Brentrup, W.S. Beck, J.A. Zwart, R. Bhattacharya, L.S. Brighenti, S.H. Burnet, I.M. McCullough, B.G. Steele, C.C. Carey, K.L. Cottingham, M.C. Dietze, H.A. Ewing, K.C. Weathers, and S.L. LaDeau. 2020. Lake Sunapee Gloeotrichia echinulata density near-term hindcasts from 2015-2016 and meteorological model driver data, including shortwave radiation and precipitation from 2009-2016 ver 4. Environmental Data Initiative. https://doi.org/DOI_PLACE_HOLDER. Accessed 2020-05-27.[3]

---

[3] This publication is currently in the staging, or draft, environment of the EDI repository. The current draft may be accessed by navigating to https://portal-s.edirepository.org/nis/home.jsp and searching for the package identifier edi 18.

Text S1: *Data processing for potential environmental drivers of G. echinulata density*

The majority of the environmental covariate data tested as potential drivers of *G. echinulata* density required processing before being used as driver data for Bayesian state-space models.

Growing degree days were calculated for each sampling day using water temperature from Onset loggers at our nearshore sampling site according to the following equation (McMaster and Wilhelm 1997):

$$\frac{(T_{max} + T_{min})}{2} - T_{base} \quad (\text{eqn. } 1)$$

where T_{max} is maximum daily temperature, T_{min} is minimum daily temperature, and T_{base} is the temperature below which *G. echinulata* cannot grow, which we assigned as $4°C$ for our calculations.

We used water temperature profiles from the GLEON buoy thermistor chain to calculate Schmidt stability, a measure of thermal stratification strength that indicates the amount of energy required to homogenize temperature across the water column (Idso 1973). Schmidt stability calculations were performed using the R package rLakeAnalyzer (Winslow et al. 2019). The 10-min. Schmidt stability data were aggregated to daily summary statistics for days where at least 75% of observations were present for that day.

Following observations that wind can promote nearshore *G. echinulata* scums by facilitating aggregation of colonies in littoral areas (Cyr 2017), wind speed and wind direction data were tested as potential environmental drivers. For 2009-2010 and 2013-2016, 10-minute averages of 1-sec. wind speed and wind direction data were aggregated to hourly means. For 2011-2012, average wind speed and wind direction were not available, so 10-min instantaneous readings were used and also aggregated to an hourly mean. Using the hourly mean wind

direction data, we added an indicator variable coded as 1 for wind directions that could feasibly have blown *G. echinulata* colonies in the direction of our study site our study site (S to NW 180-359°), while wind blowing in the opposite direction was coded as 0 (0-179°). We aggregated the hourly wind speed data to daily mean, median, minimum, maximum, and standard deviation if at least 50% of observations were present for that day. The wind direction indicator variable data were aggregated to a daily mean which ranged from 0-1 depending on the proportion of hourly wind measurements blowing towards Site 1 each day.

Hourly NLDAS-2 solar radiation data were aggregated to daily sum, mean, standard deviation, median, minimum, and maximum values.

Text S2: *Selection of environmental covariates for Bayesian state-space models*

Based on our expectations as to which environmental covariates could be important for driving *Gloeotrichia* density from our knowledge of cyanobacterial dynamics in eutrophic lakes (e.g., Barbiero and Welch 1992, Ist́vanovics et al. 1993, Karlsson-Elfgren et al. 2005, Carey et al. 2014, Cottingham et al. 2015), we performed a standardized selection process to determine which environmental covariates and summary statistics of those covariates to include in Bayesian state-space models. To select covariates, we conducted Spearman's correlations between summary statistics of candidate environmental covariates and log-transformed *G. echinulata* density between 2009 and 2014 (Table S2). We conducted correlations using multiple summary statistics of the following covariates: water temperature, Schmidt stability, precipitation, wind speed, wind direction, shortwave radiation, photosynthetically active radiation (PAR), and growing degree days. We used the Spearman's *rho* of these correlations to guide which environmental covariates and the specific summary statistic to use in developing Bayesian state-space models.

For each environmental covariate, we conducted correlations for a suite of different summary statistics, including the mean, minimum, and maximum values as well as the standard deviation of the covariate for each sampling day. We also conducted correlations for each of these summary statistics at one-day to one-week lags from the day of sampling when data permitted, as well as for the difference in an environmental covariate from one week to the next to account for antecedent conditions or rapid changes in environmental covariates, according to previous findings that antecedent conditions or changes in conditions such as water temperature and Schmidt stability can affect cyanobacterial growth and phytoplankton community structure (Bormans et al. 2005, Madgwick et al. 2006). For water temperature, we further conducted

correlations using moving averages for 3-14 days prior to each sampling day. Finally, if initial data visualization indicated that environmental covariates exhibited a quadratic relationship with log-transformed *G. echinulata* density and therefore did not meet the assumption of monotonicity for a Spearman's correlation, we used a quadratic R^2 threshold of $| R^2 | \geq 0.3$ for covariate selection; this occurred for growing degree days (Fig. S1). The full list of covariate summary statistics can be viewed in Table S2.

After completing all correlations, we assessed which environmental covariate summary statistics to include in our Bayesian state-space models using Spearman's *rho* from 2009-2014. We eliminated any covariate summary statistics for which |Spearman's *rho*| was less than 0.3. We arrived at this threshold because 0.3 was approximately twice the |mean *rho*| across all covariates (|mean *rho*| = 0.14). If multiple summary statistics for a particular environmental covariate had a |Spearman's *rho*| that was greater than or equal to 0.3, we chose the summary statistic with the greatest |Spearman's *rho*| value for Bayesian state-space model development (Table S2). For quadratic variables that did not meet the monotonicity assumption for Spearman's correlations, we used a threshold of |quadratic $R^2| \geq 0.3$ for prioritization.

Using this covariate selection process, we identified eight environmental covariate summary statistics for inclusion in Bayesian state-space models: daily minimum water temperature on the sampling day (MinWaterTemp), daily minimum water temperature with a one-week lag (MinWaterTempLag), seven-day moving average of water temperature (WaterTempMA), weekly difference in median Schmidt stability (ΔSchmidt), daily maximum Schmidt stability with a one-week lag (SchmidtLag), daily mean of the wind direction indicator variable with a two-day lag (WindDir), growing degree days (GDD), and daily sum of precipitation (Precip).

Text S3: *Random walk model and development of informed observation error prior*

Our null Bayesian state-space model was a random walk model, or a linear model with a slope of 0 and a process error term (RW; Table 1), with an informed observation error prior developed using data from Site 2 (Fig. 2). For the informed observation error prior, we used logged *G. echinulata* density data collected weekly at Site 2 in Lake Sunapee from 2009-2014 (Fig. 2) to run a random walk model with vague priors. Observation error was modeled as a normal distribution with precision τ_{obs}, which was assigned a vague gamma distribution prior with shape (a = 0.001) and rate (r = 0.001). After convergence, the model estimated the shape and rate of τ_{obs} to be 15.37 and 7.84, respectively, and these values were used for the prior on τ_{obs} in all models subsequently developed for Site 1 as part of our analysis.

Initial conditions priors for all models were informed using *G. echinulata* densities observed in north temperate lakes in Maine, U.S.A during April and May across multiple years (H. Ewing, unpublished data).

Text S4: *Model ensemble exercise*

Development of model ensemble

Following observations that model ensembles can sometimes provide more skilled predictions than a single model even when some ensemble members are low-performing (Johansson et al. 2019), we conducted a simple, unweighted model ensemble exercise to determine if the model ensemble could out-perform our individual models. We created the ensemble by appending all of the 7,500-member within-model hindcasts for each week for each model (excluding the RW null model) and conducted the same hindcast assessment and uncertainty partitioning on the grouped hindcast output as we did for individual models.

Model ensemble hindcast skill similar to individual models

The model ensemble did not perform better than the best-performing individual models, with a ΔPL of 0.05 ln(colonies L^{-1}) at the one-week forecast horizon and 0.09 ln(colonies L^{-1}) at the four-week horizon (Table 2; Fig. 5; Fig. 6; Fig. S11; Fig. S13). Overall, all models included in the ensemble exhibited a tendency to under-predict *G. echinulata* at both the one-week and four-week forecast horizon (see Bias in Table 2), likely resulting in negligible improvement in hindcast skill using an ensemble approach.

Text S5: *Variability of environmental covariates in Bayesian state-space models*

The environmental covariates selected for Bayesian state-space models were temporally variable from 2009-2016. Minimum daily water temperature at Site 1 (used in MinWaterTemp and MinWaterTempLag models) ranged from 13.4 °C to 26.2 °C and peaked between July 15 – August 20 during the study years (Fig. S2; Fig. S3). Weekly moving averages of water temperature at Site 1 (WaterTempMA model) were similar, ranging from 13.2 °C to 26.2 °C and reaching a maximum between July 11 – August 27 during the study years (Fig. S4). Growing degree days increased throughout the sampling season each year (Fig. S5).

Coinciding with summer increases in surface water temperature, Lake Sunapee was thermally stratified in all study years but did sometimes experience fall turnover (homogenization of water column temperatures) before the end of the sampling season, so daily maximum Schmidt stability (SchmidtMaxLag model) ranged from 0-695 J m^{-2} in June-October (Fig. S6). Thermal stability peaked between July 15 – August 27 in all study years. However, the weekly change in Schmidt stability (SchmidtMedDiff model and two-covariate models) varied substantially both within and among years, with some weeks displaying large increases or decreases in Schmidt stability ($\pm$ 200 J m^{-2}) while other weeks exhibited no change in stability (Fig. S7).

Precipitation (Precip model and two-covariate models) was also highly variable among years, with 2009, 2011, 2013, and 2014 all including precipitation events of 20 mm day^{-1} or more (Fig. S8). Conditions were drier in other years and 2012 was an especially dry year with a maximum daily sum of precipitation of 4.1 mm. Notably, both of the hindcasting years (2015 and 2016) were drier years.

Finally, the proportion of wind measurements blowing towards Site 1 (WindDir model

and two-covariate models) was also highly variable both within and among years, with values ranging from nearly 0 (no wind blowing towards Site 1) to nearly 1 (all wind blowing towards Site 1) on a week-to-week basis (Fig. S9). In general, wind blew towards Site 1 more often than not, with the proportion of wind measurements blowing towards Site 1 averaging 0.69 throughout the study period. However, actual wind speed was not usually very high, with wind speed in the direction of Site 1 having a median of 2.6 m s^{-1} and maximum of 6.7 m s^{-1} during the study period.

Table S1: Examples of ecological forecasts with partitioned uncertainty. These studies are provided as examples only and do not represent a systematic literature review. IC = initial conditions; SDM = species distribution model; RCP = representative concentration pathway; GCM = global climate model

Paper	Ecosystem or region	Focal forecasting variable	Forecast horizon	Type of model	Types of uncertainty quantified	Dominant source of uncertainty
(Dietze 2017)	Forest	Net ecosystem exchange	Daily	2-covariate Bayesian state-space	Driver, IC, process, parameter	Driver
(Diniz-Filho et al. 2009)	Western hemisphere	Bird population distribution	Multi- decadal	Species distribution model	Driver, process	Process
(Fox et al. 2018)	Arid woodland/ grassland	Carbon stock	Annual	Community land model	Driver, IC	IC
(Gauthier et al. 2016)	Arctic	Snow goose population	Multi- decadal	Time-varying matrix population model	Driver, parameter, process	Parameter
(Gertner et al. 1996)	Forest	Red pine growth	Multi- decadal	Pipe model (process-based)	IC, parameter	Parameter
(Huang et al. 2013)	Lake	Chlorophyll	Biweekly	Complex numerical process-based	IC, parameter	IC
(Jiang et al. 2012)	Global (high latitudes)	Vegetation distribution	Multi-decadal	Dynamic global vegetation model	Driver, parameter	Parameter
(Jiang et al. 2018)	Peatland	Carbon stocks and fluxes	Decadal	Process-based	Driver, parameter	Driver
(Kim et al. 2014)	River	Chlorophyll	Spatial	Process-based	Driver (different sources)	Driver (river flow)
(Massoud et al. 2018)	Plankton mesocosm	Plankton abundance	Daily	Process-based	IC, parameter, process	Process
(Mbogga et al. 2010)	Forest	Aspen habitat	Multi- decadal	Bioclimate envelope model	Driver, process	Driver

Paper	Ecosystem or region	Focal forecasting variable	Forecast horizon	Type of model	Types of uncertainty quantified	Dominant source of uncertainty
(Ouellet-Proulx et al. 2017)	River	Water temperature and discharge	Daily	Process-based	Driver, IC	Driver
(Page et al. 2017)	Lake	Phytoplankton community	Weekly	Complex numerical process-based	Process (different sources)	Process (representation of light, nutrients)
(Raiho et al. in review)	Forest	Tree species biomass	Multi- decadal	Process-based forest gap model	Driver, IC, parameter, process	Process
(Spadavecchia et al. 2011)	Forest	CO_2 flux	Daily	Process-based ecosystem model	Driver, parameter	Parameter
(Thomas et al. 2018)	Forest	Productivity	Decadal	Complex numerical process-based	Driver, parameter, process	Process
(Thomas et al. 2020)	Lake	Water temperature	Daily	Complex numerical process-based	Driver, IC, parameter, process	Driver
(Thuiller et al. 2019)	Global	Vertebrate species distributions	Multi-decadal	Species distribution model	Driver and process (different sources of each)	Driver (RCP scenarios) and process (choice of SDM)
(Wang et al. 2009)	Forest	Forest carbon	Spatial	Kriging algorithm	Driver (different sources)	Driver (satellite data)

Supplemental information for Lofton et al., Using near-term forecasts and uncertainty partitioning to improve predictions of low-frequency cyanobacterial events

Paper	Ecosystem or region	Focal forecasting variable	Forecast horizon	Type of model	Types of uncertainty quantified	Dominant source of uncertainty
(Watling et al. 2015)	Southeastern U.S.	Vertebrate species distribution	Multi-decadal	Species distribution model	Driver, IC, process	Process
(Valle et al. 2009)	Tropical forest	Basal area	Multi-decadal	Complex numerical process-based	IC, parameter, process	Process
(Zhang et al. 2019)	Maize fields	Crop yield	Multi-decadal	Process-based	Driver (different sources) and process	Driver (GCMs)

Table S2: Correlation analysis results to determine which environmental covariates to include in Bayesian state-space models. Variable names are provided to match variables names in the output.csv file generated by the "2A_Covariate_correlation.R" script in the manuscript's Github repository. Quadratic R^2 instead of Spearman's *r* is reported for variables which were determined to have a quadratic relationship with logged *G. echinulata* density during preliminary visualization. Shaded boxes indicate variables that met the prioritization criterion of *r* or $R^2 \geq 0.3$. Asterisks indicate variables chosen for inclusion in Bayesian state-space models. P-values have been adjusted using the Holm-Bonferroni correction to account for multiple comparisons except in the case of growing degree days, where the p-value is for quadratic regression rather than a Spearman's correlation.

Covariate variable name	Covariate variable description	Spearman's *rho*	Quadratic reg. R^2	p-value
HCS.tempC_mean	mean water temperature on the sampling day	0.49	--	6.9×10^{-6}
HCS.tempC_median	median water temperature on the sampling day	0.49	--	8.5×10^{-6}
HCS.tempC_min	minimum water temperature on the sampling day	0.51	--	2.1×10^{-6}
HCS.tempC_max	maximum water temperature on the sampling day	0.47	--	2.5×10^{-5}
HCS.tempC_sd	standard deviation of water temperature on the sampling day	-0.17	--	1
HCS.tempC_mean_lag	daily mean water temperature one week before the sampling day	0.54	--	2.1×10^{-7}
HCS.tempC_median_lag	daily median water temperature one week before the sampling day	0.54	--	1.6×10^{-7}
HCS.tempC_min_lag	daily minimum water temperature one week before the sampling day	0.56*	--	4.2×10^{-8}
HCS.tempC_max_lag	daily maximum water temperature one week before the sampling day	0.52	--	6.2×10^{-7}
HCS.tempC_sd_lag	daily standard deviation of water temperature one week before the sampling day	-0.19	--	1
wtr_mean_diff	difference in mean water temperature between one week before the sampling day and the day of sampling	-0.2	--	1
wtr_median_diff	difference in median water temperature between one week before the sampling day and the day of sampling	-0.2	--	1

Covariate variable name	Covariate variable description	Spearman's *rho*	Quadratic reg. R^2	p-value
wtr_max_diff	difference in maximum water temperature between one week before the sampling day and the day of sampling	-0.18	--	1
wtr_min_diff	difference in minimum water temperature between one week before the sampling day and the day of sampling	-0.2	--	1
wtr_sd_diff	difference in standard deviation in water temperature between one week before the sampling day and the day of sampling	-0.02	--	1
ma_3	three-day moving average of water temperature prior to the day of sampling	0.44	--	0.00022
ma_5	five-day moving average of water temperature prior to the day of sampling	0.45	--	0.00013
ma_7	seven-day moving average of water temperature prior to the day of sampling	0.49*	--	1.7×10^{-5}
ma_10	ten-day moving average of water temperature prior to the day of sampling	0.44	--	0.00052
ma_14	fourteen-day moving average of water temperature prior to the day of sampling	0.48	--	5.0×10^{-5}
gdd_sum	growing degree days	--	0.52*	1.2×10^{-17}
schmidt.stability_mean	mean Schmidt stability on the day of sampling	0.19	--	1
schmidt.stability_median	median Schmidt stability on the day of sampling	0.19	--	1
schmidt.stability_min	minimum Schmidt stability on the day of sampling	0.18	--	1
schmidt.stability_max	maximum Schmidt stability on the day of sampling	0.2	--	1
schmidt.stability_sd	standard deviation of Schmidt stability on the day of sampling	0.19	--	1
schmidt.stability_mean_lag	daily mean Schmidt stability one week before the sampling day	0.35	--	0.025
schmidt.stability_median_lag	daily median Schmidt stability one week before the sampling day	0.35	--	0.022
schmidt.stability_min_lag	daily minimum Schmidt stability one week before the sampling day	0.34	--	0.047

Covariate variable name	Covariate variable description	Spearman's *rho*	Quadratic reg. R^2	p-value
schmidt.stability_max_lag	daily maximum Schmidt stability one week before the sampling day	0.36*	--	0.015
schmidt.stability_sd_lag	daily standard deviation of Schmidt stability one week before the sampling day	0.13	--	1
schmidt.stability_mean_diff	difference in mean Schmidt stability between one week before the sampling day and the day of sampling	-0.34	--	0.05
schmidt.stability_median_diff	difference in median Schmidt stability between one week before the sampling day and the day of sampling	-0.36*	--	0.02
schmidt.stability_min_diff	difference in minimum Schmidt stability between one week before the sampling day and the day of sampling	-0.3	--	0.20
schmidt.stability_max_diff	difference in maximum Schmidt stability between one week before the sampling day and the day of sampling	-0.34	--	0.05
schmidt.stability_sd_diff	difference in standard deviation of Schmidt stability between one week before the sampling day and the day of sampling	-0.05	--	1
precip_mm	sum of daily precipitation on day of sampling	-0.3*	--	0.05
precip_mm_1daylag	sum of daily precipitation on day before sampling	-0.23	--	0.73
precip_mm_1weeklag	sum of daily precipitation one week before the sampling day	-0.22	--	0.89
ShortWaveRad_Wperm2_mean	mean shortwave radiation on the day of sampling	0.04	--	1
ShortWaveRad_Wperm2_median	median shortwave radiation on the day of sampling	-0.21	--	1
ShortWaveRad_Wperm2_min	minimum shortwave radiation on the day of sampling	0.27	--	0.16
ShortWaveRad_Wperm2_max	maximum shortwave radiation on the day of sampling	0.07	--	1
ShortWaveRad_Wperm2_sd	standard deviation of shortwave radiation on the day of sampling	0.11	--	1
ShortWaveRad_Wperm2_sum	sum of shortwave radiation on the day of sampling	0.04	--	1
par_mean	mean PAR on the day of sampling	0	--	1
par_median	median PAR on the day of sampling	-0.21	--	1
par_min	minimum PAR on the day of sampling	0.16	--	1

Covariate variable name	Covariate variable description	Spearman's *rho*	Quadratic reg. R^2	p-value
par_max	maximum PAR on the day of sampling	-0.03	--	1
par_sd	standard deviation of PAR on the day of sampling	0.08	--	1
par_sum	sum of PAR on the day of sampling	0	--	1
AveWindSp_ms_mean_in	mean windspeed filtered for wind directions blowing into Site 1 on the day of sampling	0.08	--	1
AveWindSp_ms_median_in	median windspeed filtered for wind directions blowing into Site 1 on the day of sampling	0.09	--	1
AveWindSp_ms_min_in	minimum windspeed filtered for wind directions blowing into Site 1 on the day of sampling	0.16	--	1
AveWindSp_ms_max_in	maximum windspeed filtered for wind directions blowing into Site 1 on the day of sampling	0.03	--	1
AveWindSp_ms_sd_in	standard deviation of windspeed filtered for wind directions blowing into Site 1 on the day of sampling	0.01	--	1
AveWindSp_ms_mean_1daylag_in	mean windspeed filtered for wind directions blowing into Site 1 the day before the sampling day	0.13		1
AveWindSp_ms_median_1daylag_in	median windspeed filtered for wind directions blowing into Site 1 the day before the sampling day	0.15	--	1
AveWindSp_ms_min_1daylag_in	minimum windspeed filtered for wind directions blowing into Site 1 the day before the sampling day	0.14	--	1
AveWindSp_ms_max_1daylag_in	maximum windspeed filtered for wind directions blowing into Site 1 the day before the sampling day	0.13	--	1
AveWindSp_ms_sd_1daylag_in	standard deviation of windspeed filtered for wind directions blowing into Site 1 the day before the sampling day	0.16	--	1
AveWindSp_ms_mean_2daylag_in	mean windspeed filtered for wind directions blowing into Site 1 two days before the sampling day	0.25	--	0.50
AveWindSp_ms_median_2daylag_in	median windspeed filtered for wind directions blowing into Site 1 two days before the sampling day	0.26	--	0.46

Covariate variable name	Covariate variable description	Spearman's rho	Quadratic reg. R²	p-value
AveWindSp_ms_min_2daylag_in	minimum windspeed filtered for wind directions blowing into Site 1 two days before the sampling day	0.29	--	0.14
AveWindSp_ms_max_2daylag_in	maximum windspeed filtered for wind directions blowing into Site 1 two days before the sampling day	0.23	--	0.95
AveWindSp_ms_sd_2daylag_in	standard deviation of windspeed filtered for wind directions blowing into Site 1 two days before the sampling day	0.2	--	1
AveWindSp_ms_mean_3daylag_in	mean windspeed filtered for wind directions blowing into Site 1 three days before the sampling day	0.23	--	0.95
AveWindSp_ms_median_3daylag_in	median windspeed filtered for wind directions blowing into Site 1 three days before the sampling day	0.24	--	0.67
AveWindSp_ms_min_3daylag_in	minimum windspeed filtered for wind directions blowing into Site 1 three days before the sampling day	0.26	--	0.46
AveWindSp_ms_max_3daylag_in	maximum windspeed filtered for wind directions blowing into Site 1 three days before the sampling day	0.19	--	1
AveWindSp_ms_sd_3daylag_in	standard deviation of windspeed filtered for wind directions blowing into Site 1 three days before the sampling day	0.11		1
AveWindSp_ms_mean_1weeklag_in	mean windspeed filtered for wind directions blowing into Site 1 one week before the sampling day	0.08	--	1
AveWindSp_ms_median_1weeklag_in	median windspeed filtered for wind directions blowing into Site 1 one week before the sampling day	0.09	--	1
AveWindSp_ms_min_1weeklag_in	minimum windspeed filtered for wind directions blowing into Site 1 one week before the sampling day	0.13	--	1
AveWindSp_ms_max_1weeklag_in	maximum windspeed filtered for wind directions blowing into Site 1 one week before the sampling day	0.04	--	1
AveWindSp_ms_sd_1weeklag_in	standard deviation of filtered for wind directions blowing into Site 1 one week before the sampling day	0.03	--	1
windsp_cumsum_1day_in	cumulative windspeed into the cove one day prior to sampling	0.09	--	1

Covariate variable name	Covariate variable description	Spearman's *rho*	Quadratic reg. R^2	p-value
windsp_cumsum_2day_in	cumulative windspeed into the cove two days prior to sampling	0.13	--	1
AveWindDir_cove_mean	proportion of daily wind measurements blowing in the direction of Site 1 on the day of sampling	0.2	--	1
AveWindDir_cove_mean_1daylag	proportion of daily wind measurements blowing in the direction of Site 1 one day before sampling	0.19	--	1
AveWindDir_cove_mean_2daylag	proportion of daily wind measurements blowing in the direction of Site 1 two days before sampling	0.37*	--	0.0072
AveWindDir_cove_mean_3daylag	proportion of daily wind measurements blowing in the direction of Site 1 three days before sampling	0.2		1
AveWindDir_cove_mean_1weeklag	proportion of daily wind measurements blowing in the direction of Site 1 on the day one week before sampling	0.11	--	1

Table S3: Estimated mean random year effects for calibrated random walk model with random year effect from 2009-2014. The model parameter τ_{year} was estimated to have a mean of 64.8, corresponding to a standard deviation of 0.12 being fit to the mean random year effects reported in the table.

Year	*2009*	*2010*	*2011*	*2012*	*2013*	*2014*
Mean random year effect	0.069	0.026	0.002	0.026	0.058	0.038

Table S4: Parameter summary for all calibrated Bayesian state-space models: Part I. Model process equations and descriptions of covariates included in each model can be found in Table 1 of the manuscript. Parameter names are provided to match output from R script "4.2_Calibrate_Bayesian_models.R" included as part of the GitHub code repository for this manuscript. tau_proc = precision on the normal distribution representing process error; tau_obs = precision on the normal distribution representing observation error; beta1 = intercept of linear models; beta2 = coefficient of AR term in linear models; S.D. = standard deviation; PSRF = potential scale reduction factor of the Gelman-Rubin statistic, sometimes referred to as R-hat, where a value approaching 1 indicates that the model has converged well on a parameter estimate both within and among chains; SS_{eff} = effective sample size, or the number of independent samples in MCMC output for a parameter once auto-correlation has been accounted for.

Parameters	tau_proc				tau_obs				beta1				beta2			
Model name	mean	S.D.	PSRF	SS_{eff}	mean	S.D.	PSRF	SS_{eff}	mean	S.D.	PSRF	SS_{eff}	mean	S.D.	PSRF	SS_{eff}
RW	0.70	0.16	1.00	21851	1.72	0.35	1.00	20044	--	--	--	--	--	--	--	--
AR	0.75	0.17	1.00	18748	1.80	0.37	1.00	18302	-0.26	0.15	1.00	33346	0.76	0.06	1.00	29639
MinWaterTemp	0.93	0.25	1.00	12612	1.72	0.36	1.00	16302	-0.39	0.15	1.00	26303	0.68	0.06	1.00	22165
MinWaterTempLag	0.85	0.21	1.00	16316	1.76	0.37	1.00	16918	-0.47	0.16	1.00	22452	0.63	0.07	1.00	18484
WaterTempMA	0.88	0.23	1.00	14034	1.75	0.37	1.00	17074	-0.39	0.15	1.00	25093	0.66	0.07	1.00	19928
ΔSchmidt	0.74	0.17	1.00	18662	1.89	0.38	1.00	18809	-0.29	0.16	1.00	27059	0.74	0.07	1.00	22980
SchmidtLag	0.89	0.23	1.00	13929	1.73	0.36	1.00	16797	-0.31	0.14	1.00	30254	0.75	0.06	1.00	24900
WindDir	0.84	0.20	1.00	16802	1.76	0.37	1.00	18279	-0.34	0.15	1.00	31447	0.72	0.06	1.00	27858
Precip	0.74	0.17	1.00	18898	1.80	0.37	1.00	18829	-0.27	0.15	1.00	31476	0.76	0.06	1.00	26990
GDD	0.92	0.28	1.00	7849	1.74	0.38	1.00	13033	0.16	0.19	1.00	19188	0.67	0.10	1.00	7888
Schmidt+Temp	0.87	0.21	1.00	15352	1.76	0.38	1.00	16282	-0.45	0.16	1.00	21287	0.62	0.07	1.00	17198
Schmidt+Precip	0.73	0.16	1.00	19113	1.80	0.37	1.00	18498	-0.30	0.16	1.00	26737	0.74	0.07	1.00	22744
Temp+Precip	0.86	0.21	1.00	15752	1.77	0.37	1.00	17294	-0.41	0.15	1.00	25870	0.65	0.07	1.00	20824
Precip+GDD	0.90	0.26	1.00	8985	1.75	0.38	1.00	14309	0.14	0.19	1.00	19120	0.65	0.10	1.00	8296

Table S5: Parameter summary for all calibrated Bayesian state-space models: Part II. Model process equations and descriptions of covariates included in each model can be found in Table 1 of the manuscript. Parameter names are provided to match output from R script "4.2_Calibrate_Bayesian_models.R" included as part of the Github code repository for this manuscript. beta3 = coefficient of covariate in single-covariate models and coefficient on first covariate, which is the first covariate in the model name, in two-covariate models; beta4 = coefficient on quadratic term for growing degree days in GDD model and coefficient on second covariate in two-covariate models; beta5 = coefficient on quadratic term for growing degree days in WindAndGDD model; S.D. = standard deviation; PSRF = potential scale reduction factor of the Gelman-Rubin statistic, sometimes referred to as R-hat, where a value approaching 1 indicates that the model has converged well on a parameter estimate both within and among chains; SS_{eff} = effective sample size, or the number of independent samples in MCMC output for a parameter once auto-correlation has been accounted for.

Parameters	beta3				beta4				beta5			
Model name	mean	S.D.	PSRF	SS_{eff}	mean	S.D.	PSRF	SS_{eff}	mean	S.D.	PSRF	SS_{eff}
RW	--	--	--	--	--	--	--	--	--	--	--	--
AR	--	--	--	--	--	--	--	--	--	--	--	--
MinWaterTemp	0.49	0.13	1.00	38491	--	--	--	--	--	--	--	--
MinWaterTempLag	0.49	0.14	1.00	27828	--	--	--	--	--	--	--	--
WaterTempMA	0.47	0.13	1.00	33718	--	--	--	--	--	--	--	--
ΔSchmidt	-0.09	0.16	1.00	31738	--	--	--	--	--	--	--	--
SchmidtLag	0.36	0.12	1.00	52607	--	--	--	--	--	--	--	--
WindDir	0.42	0.15	1.00	37608	--	--	--	--	--	--	--	--
Precip	-0.08	0.14	1.00	44501	--	--	--	--	--	--	--	--
GDD	0.20	0.19	1.00	8919	-0.58	0.17	1.00	10260	--	--	--	--
Schmidt+Temp	-0.17	0.15	1.00	28500	0.49	0.13	1.00	30182	--	--	--	--
Schmidt+Precip	-0.09	0.16	1.00	31519	-0.07	0.14	1.00	45272	--	--	--	--
Temp+Precip	0.47	0.13	1.00	35021	-0.09	0.13	1.00	43088	--	--	--	--
Precip+GDD	-0.10	0.13	1.00	41062	0.21	0.19	1.00	9751	-0.59	0.17	1.00	11474

Supplemental information for Lofton et al., Using near-term forecasts and uncertainty partitioning to improve predictions of low-frequency cyanobacterial events

Table S6: Uncertainty partitioning results across models for one-week-ahead hindcasts during the 2015-2016 hindcasting period. Mean, minimum (Min.) and maximum (Max.) proportional contributions of initial conditions, parameter, driver, and process uncertainty to hindcasting confidence intervals are reported for each model. Note the RW model does not have parameter or driver uncertainty because the model structure does not include parameters or drivers; similarly, the AR model does not include drivers. *Because contributions of parameter and driver error were so small, the estimated confidence intervals including parameter and/or driver error were occasionally smaller than those without due to numerical approximation error, leading to an estimation of "negative" parameter/driver error; this should be interpreted as no contribution of parameter/driver error, and negative parameter/driver error values were set to zero.

Model name	Initial conditions			Parameter			Driver			Process		
	Mean	Min.	Max.	Mean	Min.	Max.	Mean	Min.	Max.	Mean	Min.	Max.
RW	0.27	0.01	0.58	--	--	--	--	--	--	0.73	0.42	0.99
AR	0.18	0	0.41	0.02	0.01	0.04	--	--	--	0.8	0.56	0.96
MinWaterTemp	0.15	0	0.35	0.03	0.01	0.06	0.05	0	0.15	0.77	0.6	0.87
MinWaterTempLag	0.13	0	0.3	0.03	0.01	0.07	0.04	0	0.14	0.81	0.63	0.94
WaterTempMA	0.14	0	0.34	0.03	0.01	0.07	0.03	0	0.14	0.8	0.6	0.93
ΔSchmidt	0.17	0	0.42	0.03	0.01	0.07	0.01	0	0.03	0.79	0.54	0.96
SchmidtLag	0.19	0	0.43	0.03	0.01	0.06	0.03	0	0.08	0.76	0.54	0.95
WindDir	0.16	0	0.38	0.02	0.01	0.05	0.06	0.01	0.12	0.75	0.54	0.89
Precip	0.17	0	0.41	0.02	0.01	0.04	0.01	0	0.08	0.79	0.55	0.96
GDD	0.16	0	0.37	0.04	0*	0.07	0.01	0	0.04	0.8	0.62	0.94
Schmidt+Temp	0.13	0	0.31	0.04	0.02	0.08	0.04	0	0.12	0.79	0.63	0.92
Schmidt+Precip	0.17	0	0.4	0.03	0.01	0.08	0.02	0	0.08	0.79	0.56	0.95
Temp+Precip	0.14	0	0.33	0.03	0.02	0.07	0.04	0	0.15	0.79	0.62	0.93
Precip+GDD	0.15	0	0.36	0.05	0.02	0.09	0.02	0	0.11	0.78	0.58	0.93
Ensemble	0.18	0.03	0.4	0.03	0.02	0.05	0.03	0*	0.07	0.76	0.57	0.86

Table S7: Uncertainty partitioning results across models for four-week-ahead hindcasts during the 2015-2016 hindcasting period. Mean, minimum (Min.) and maximum (Max.) proportional contributions of initial conditions, parameter, driver, and process uncertainty to hindcasting confidence intervals are reported for each model. Note the RW model does not have parameter or driver uncertainty because the model structure does not include parameters or drivers; similarly, the AR model does not include drivers.

Model name	Initial conditions			Parameter			Driver			Process		
	Mean	Min.	Max.	Mean	Min.	Max.	Mean	Min.	Max.	Mean	Min.	Max.
RW	0.09	0	0.26	--	--	--	--	--	--	0.91	0.74	1
AR	0.02	0	0.06	0.05	0.04	0.08	--	--	--	0.93	0.87	0.95
MinWaterTemp	0.01	0	0.03	0.06	0.03	0.1	0.07	0.01	0.15	0.86	0.79	0.93
MinWaterTempLag	0.01	0	0.02	0.05	0.03	0.09	0.06	0.01	0.12	0.88	0.81	0.94
WaterTempMA	0.01	0	0.02	0.06	0.03	0.1	0.06	0.02	0.1	0.88	0.84	0.93
ΔSchmidt	0.02	0	0.06	0.06	0.04	0.09	0.01	0	0.02	0.91	0.86	0.94
SchmidtLag	0.02	0	0.06	0.06	0.03	0.09	0.09	0.02	0.21	0.83	0.73	0.92
WindDir	0.02	0	0.05	0.05	0.03	0.08	0.06	0.02	0.1	0.88	0.83	0.92
Precip	0.02	0	0.06	0.05	0.04	0.08	0.01	0	0.06	0.92	0.87	0.95
GDD	0.01	0	0.03	0.08	0.06	0.13	0.01	0	0.04	0.89	0.85	0.93
Schmidt+Temp	0.01	0	0.02	0.06	0.04	0.09	0.07	0.02	0.14	0.86	0.79	0.93
Schmidt+Precip	0.02	0	0.05	0.06	0.04	0.09	0.02	0	0.07	0.9	0.86	0.94
Temp+Precip	0.01	0	0.02	0.05	0.04	0.1	0.07	0.03	0.13	0.87	0.8	0.93
Precip+GDD	0.01	0	0.04	0.09	0.06	0.15	0.03	0	0.11	0.87	0.81	0.92
Ensemble	0.06	0.02	0.13	0.06	0.04	0.08	0.04	0.01	0.07	0.85	0.79	0.9
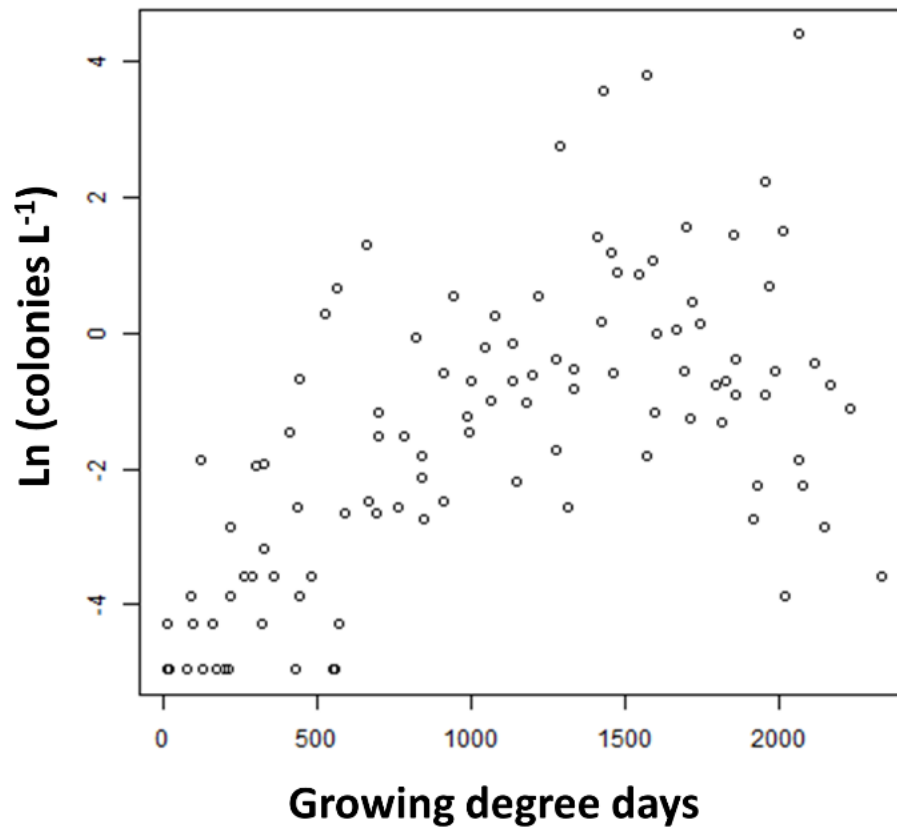
Figure S1: Natural log-transformed *G. echinulata* colonies L^{-1} vs. growing degree days for all sampling days from 2009-2016.
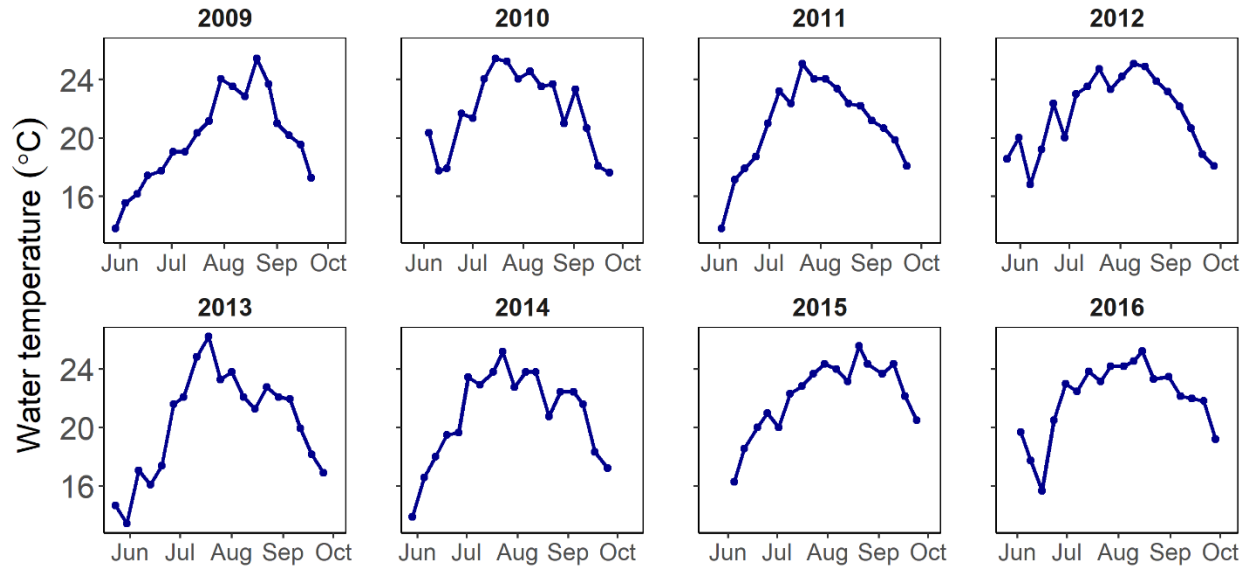
Figure S2: Timeseries of minimum water temperature at Site 1 on the day of sampling from 2009-2016.
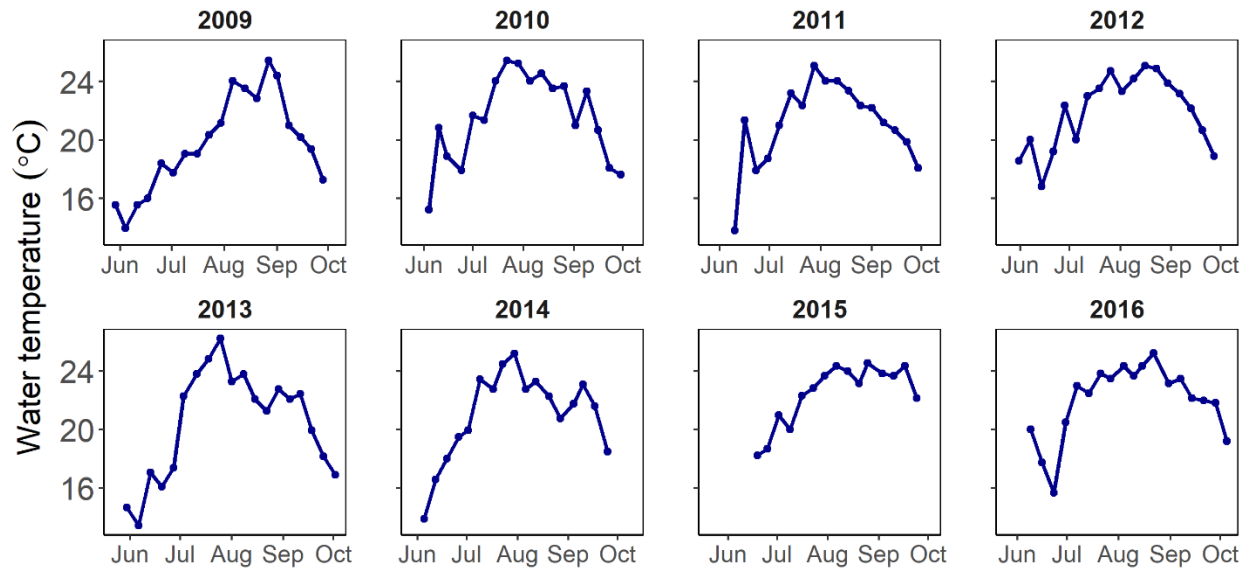
Figure S3: Timeseries of minimum water temperature at Site 1 one week before the sampling day (one week lag) from 2009-2016.
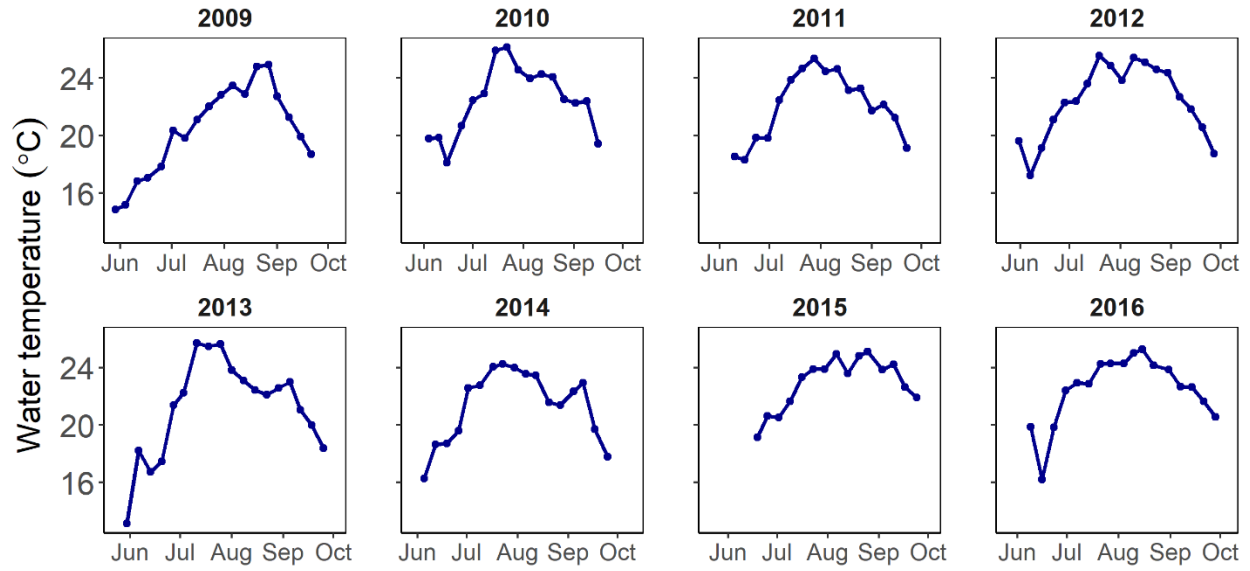
Figure S4: Timeseries of seven-day moving average of water temperature prior to the day of sampling at Site 1 from 2009-2016.
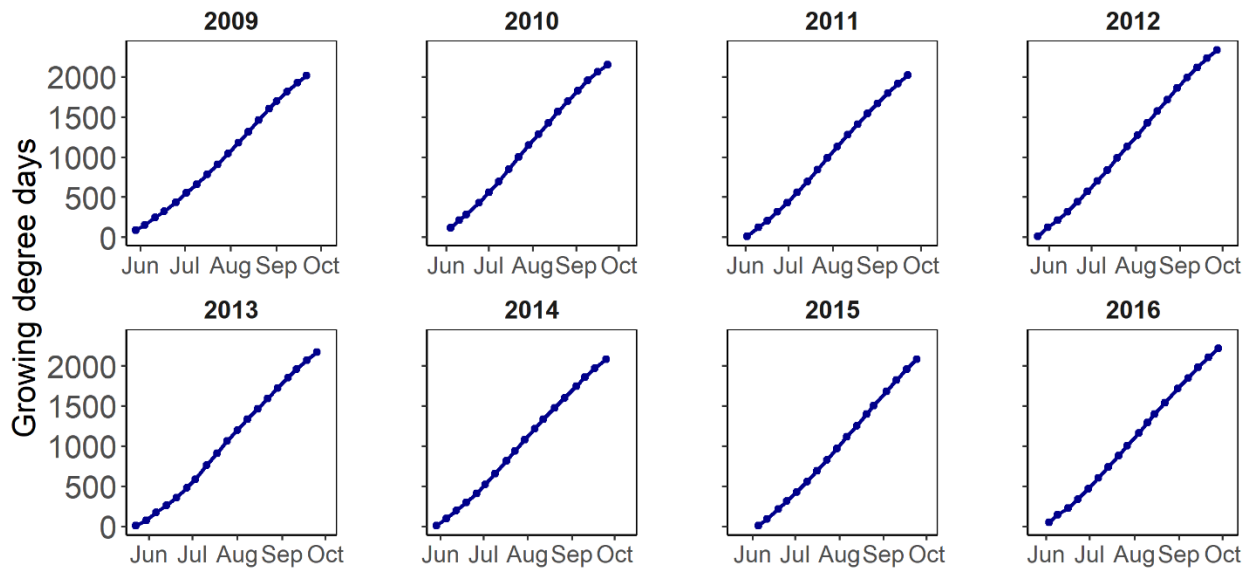
Figure S5: Timeseries of water temperature growing degree days at Site 1 from 2009-2016.
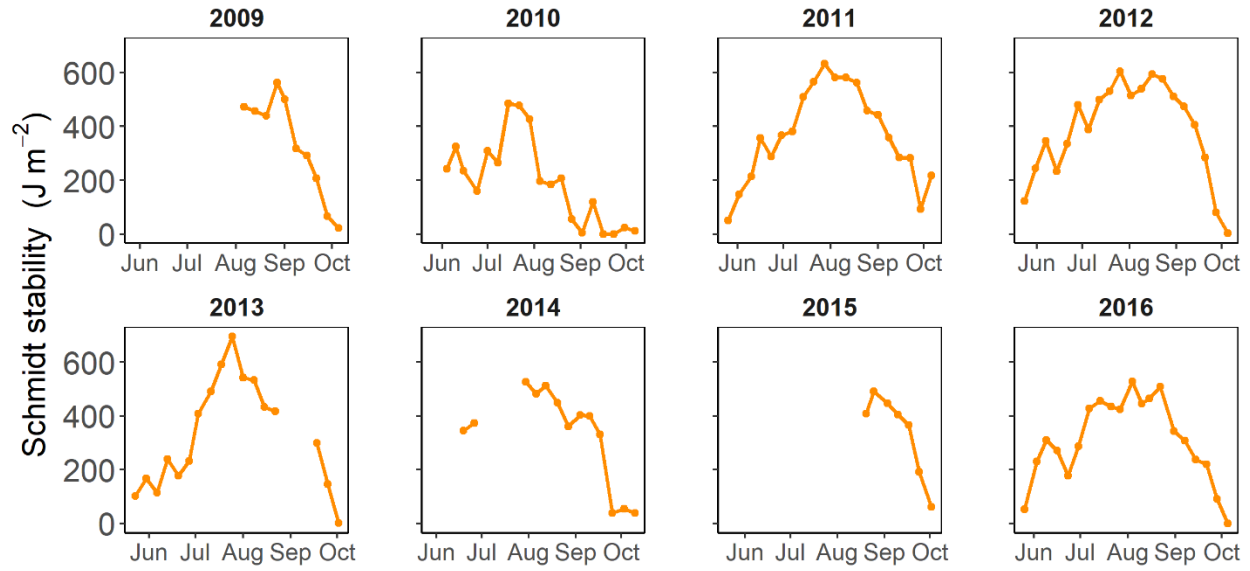
Figure S6: Timeseries of maximum Schmidt stability one week before the sampling day (one week lag) from 2009-2016.
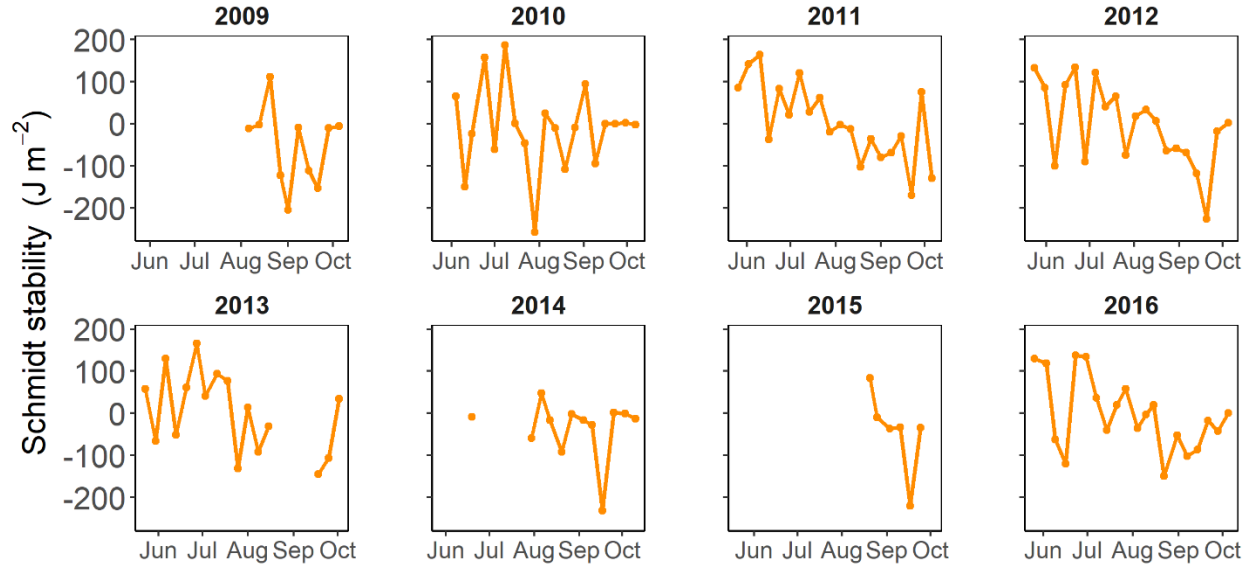
Figure S7: Timeseries of difference in median Schmidt stability between one week before the sampling day and the sampling day from 2009-2016.

Supplemental information for Lofton et al., Using near-term forecasts and uncertainty partitioning to improve predictions of low-frequency cyanobacterial events
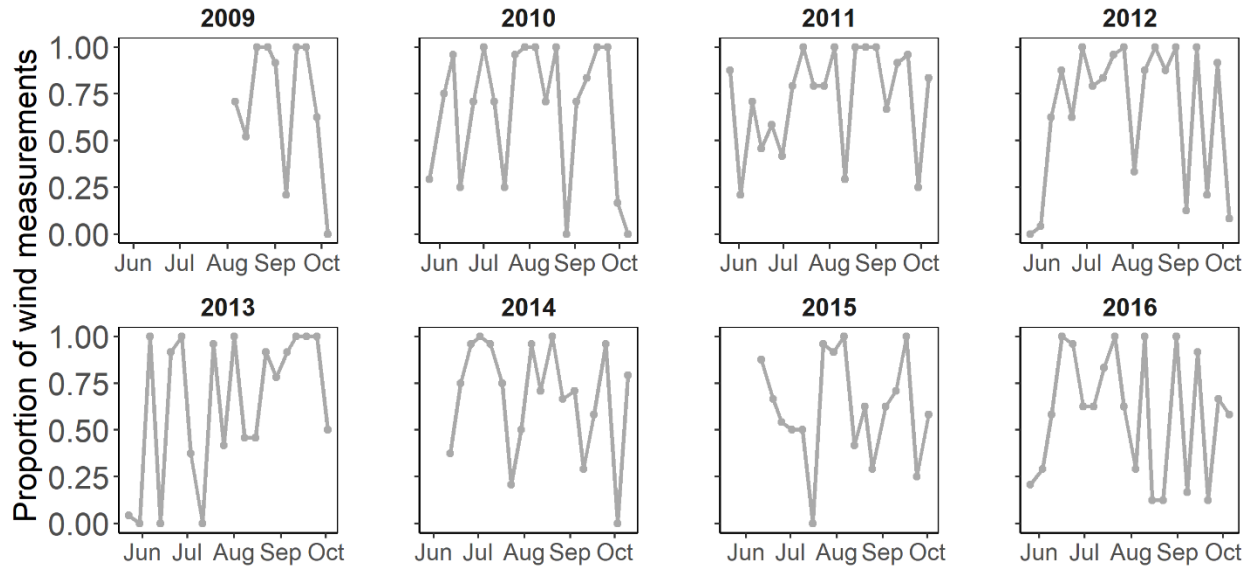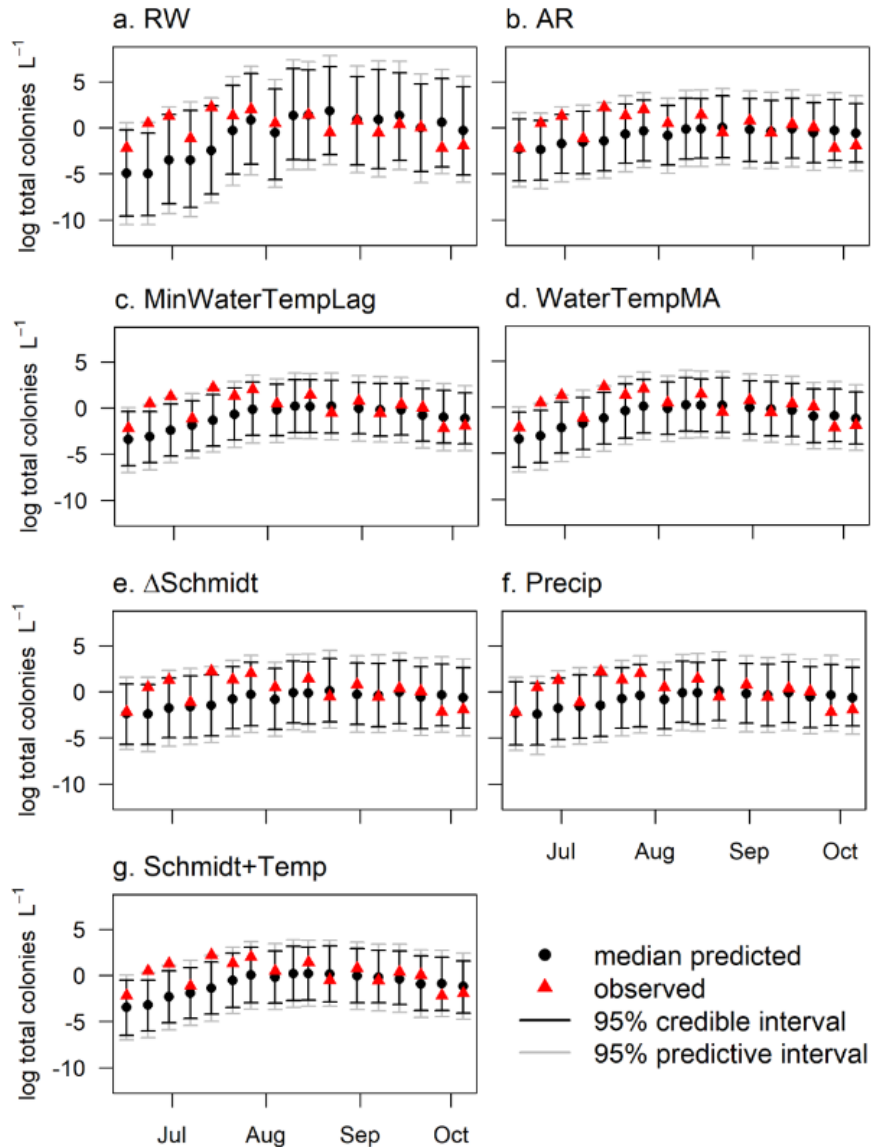

Figure S8: Timeseries of proportion of daily wind measurements blowing in the direction of Site 1 two days before the sampling day from 2009-2016.
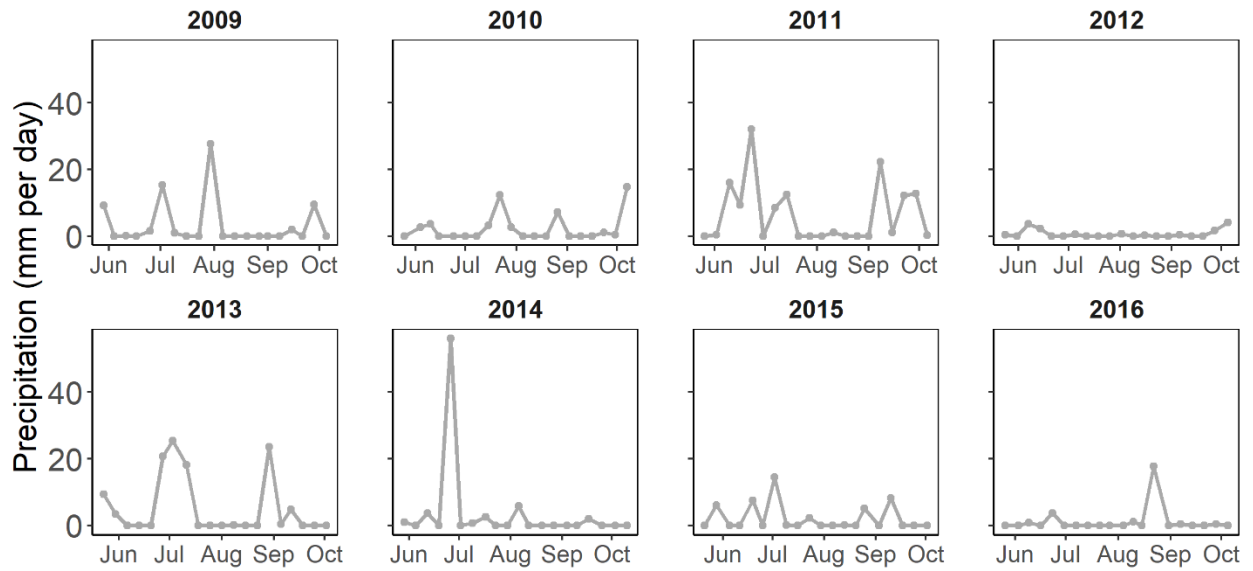
Figure S9: Timeseries of summed daily precipitation on Lake Sunapee from 2009-2016.
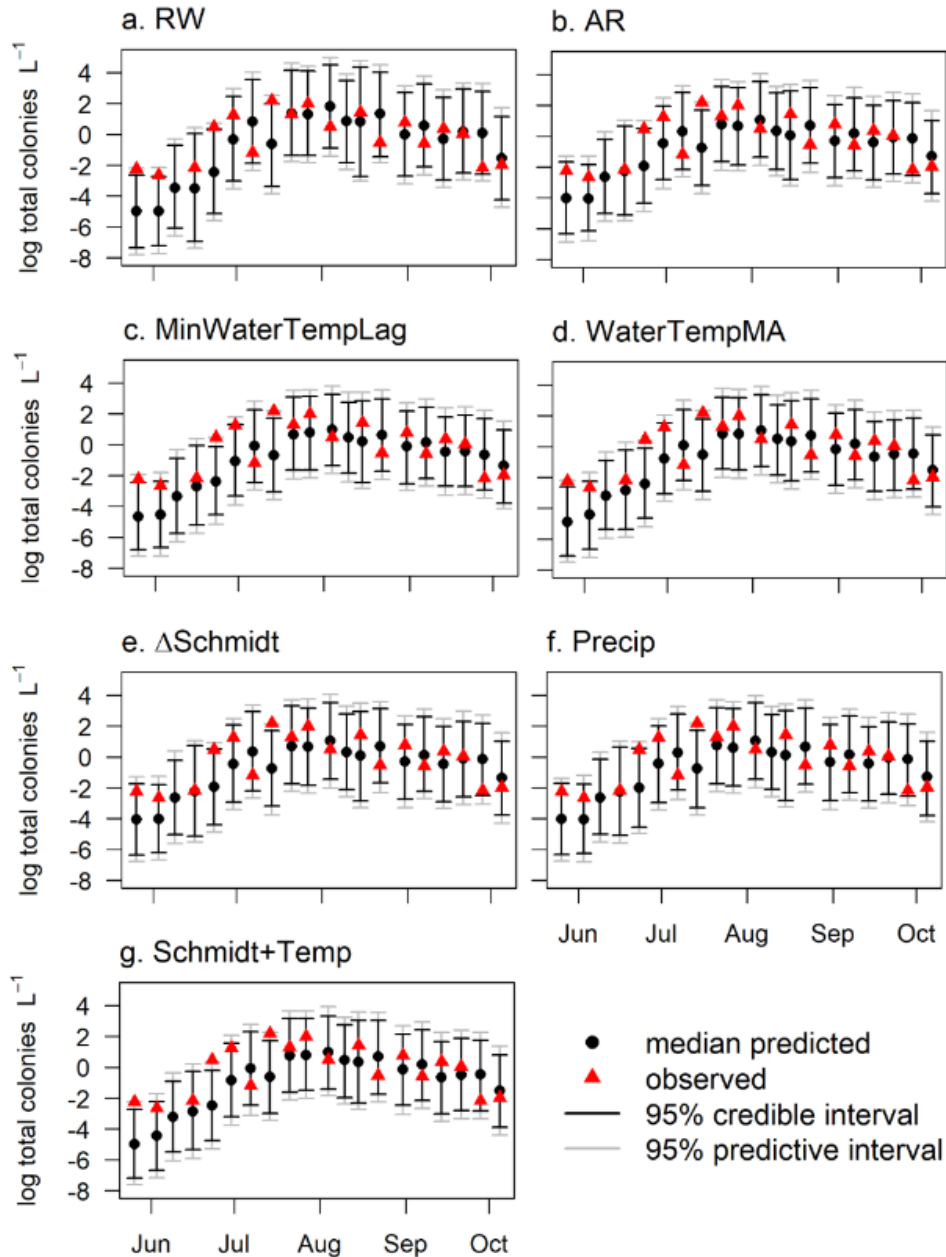
Figure S10: Timeseries of median predicted and observed *G. echinulata* density for one-week-ahead hindcasts in 2016 for the best-performing models (b-g), as well as the RW null model (a).

Figure S11 (next page): Timeseries of median predicted and observed *G. echinulata* density for one-week-ahead hindcasts in 2015 (a, c, e, g, i, k, m, o) and 2016 (b, d, f, h, j, l, n, p) for a subset of developed models. Black points are median predicted values and red triangles and observed values. Black error bars denote the 95% confidence interval, while gray error bars denote the 95% predictive interval. Models shown are MinWaterTemp (a, b), SchmidtLag (c, d), WindDir (e, f), GDD (g, h), Schmidt+Precip (i, j), Temp+Precip (k, l), Precip+GDD (m, n), and the model Ensemble (o, p).

●   median predicted

▲   observed

—   95% credible interval

—   95% predictive interval

Figure S12: Timeseries of median predicted and observed *G. echinulata* density for four-week-ahead hindcasts in 2016 for the best-performing models (b-g), as well as the RW null model (a). Note the y-axis change from Figure S10 to accommodate larger credible and predictive intervals at the four-week forecast horizon.

Figure S13 (next page): Timeseries of median predicted and observed *G. echinulata* density for four-week-ahead hindcasts in 2015 (a, c, e, g, i, k, m, o) and 2016 (b, d, f, h, j, l, n, p) for a subset of developed models. Black points are median predicted values and red triangles and observed values. Black error bars denote the 95% confidence interval, while gray error bars denote the 95% predictive interval. Models shown are MinWaterTemp (a, b), SchmidtLag (c, d), WindDir (e, f), GDD (g, h), Schmidt+Precip (i, j), Temp+Precip (k, l), Precip+GDD (m, n), and the model Ensemble (o, p). Note the y-axis change from Figure S11.
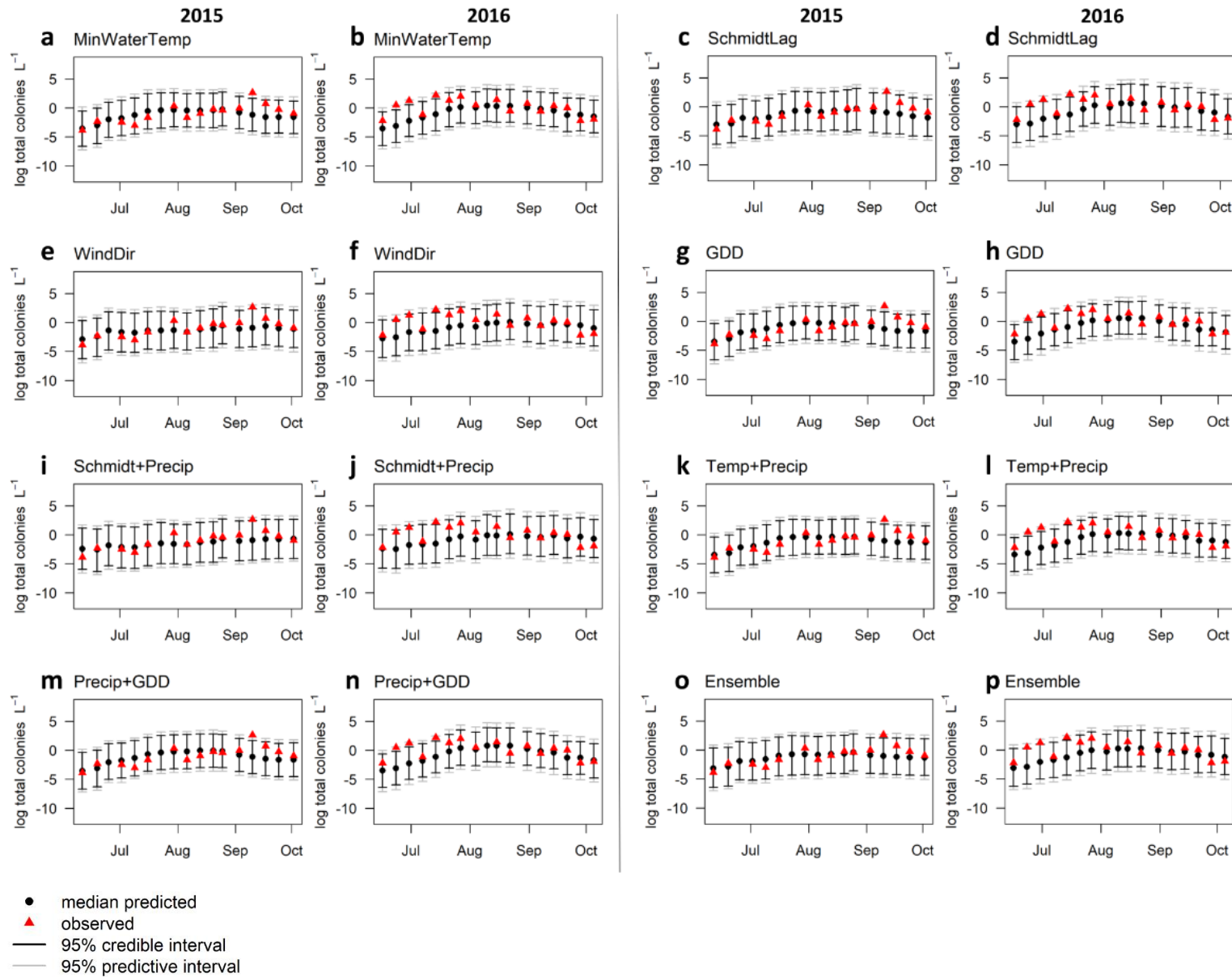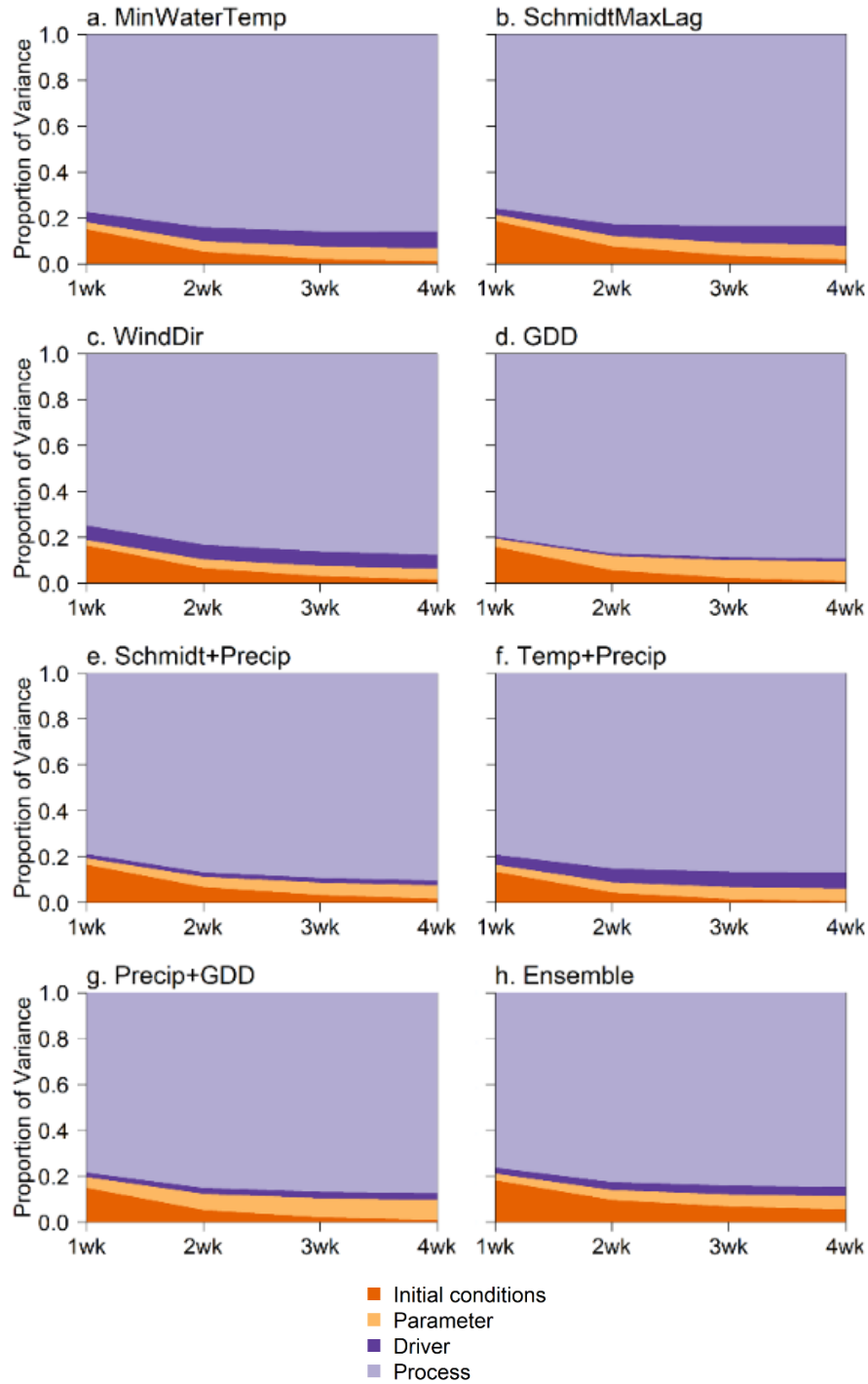
Figure S14: Uncertainty partitioning of the one-week-ahead to four-week-ahead confidence interval for hindcasts averaged across the 2015-2016 hindcasting period for eight models: a) MinWaterTemp, b) SchmidtLag, c) WindDir, d) GDD, e) Schmidt+Precip, f) Temp+Precip, g) Precip+GDD, and h) the model Ensemble.
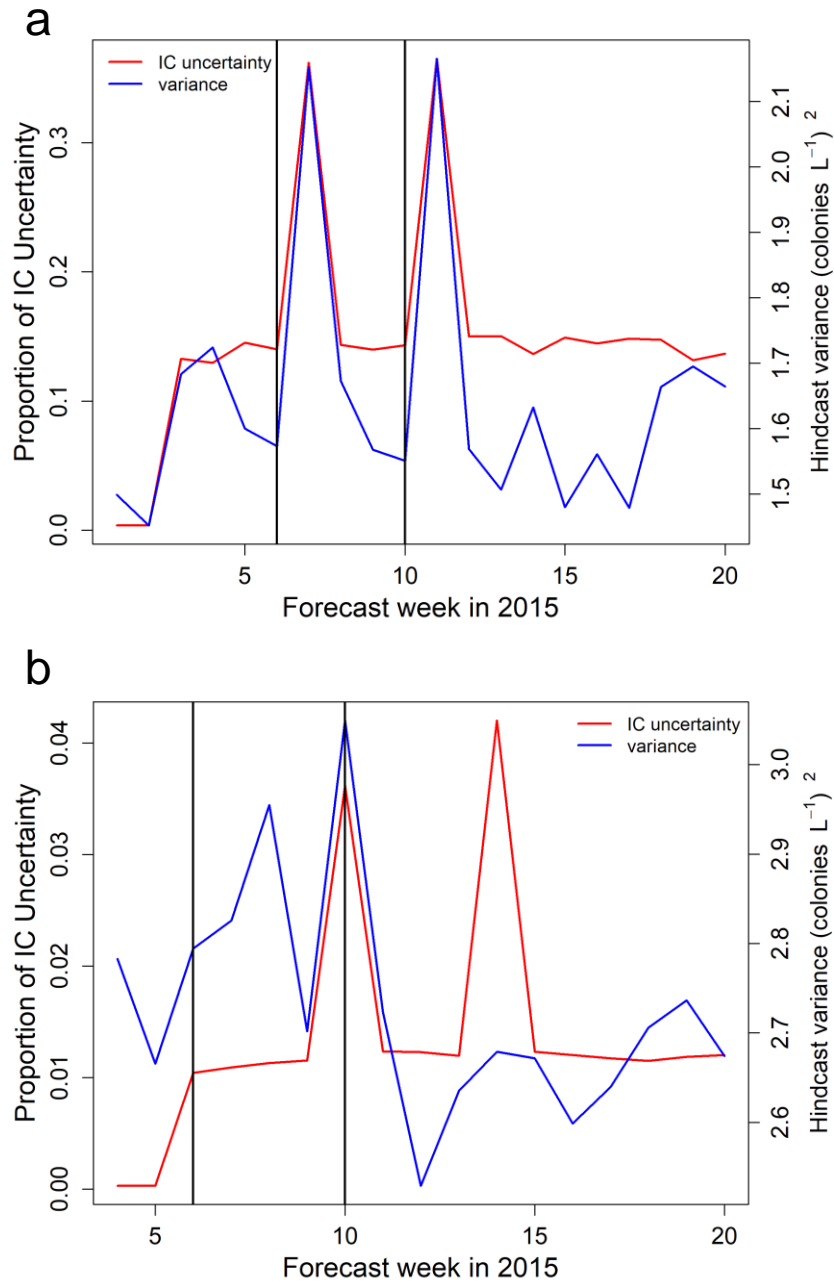
Figure S15: Hindcast variance and proportional contribution of initial contributions uncertainty to the confidence interval of during the 2015 sampling season for an example model (WindDir) for a) one-week-ahead and b) four-week-ahead forecast horizons. Vertical black lines denote times when observational *G. echinulata* data was missing during 2015. Other models exhibit the same pattern.
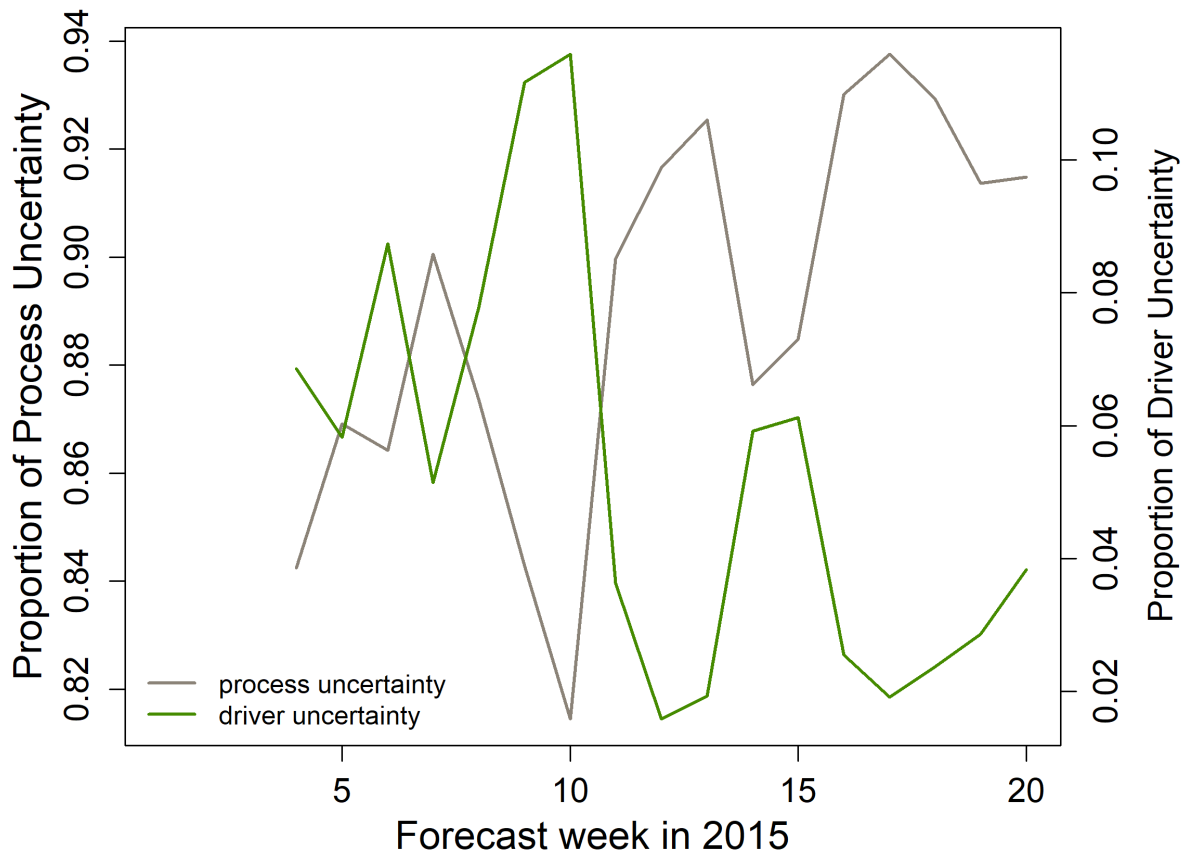
Figure S16: Relative contributions of process and driver uncertainty to total hindcast uncertainty over time for the MinWaterTempLag model in 2015.

References

Barbiero, R. P., and E. B. Welch. 1992. Contribution of benthic blue-green algal recruitment to lake populations and phosphorus translocation. Freshwater Biology 27:249–260.

Bormans, M., P. W. Ford, and L. Fabbro. 2005. Spatial and temporal variability in cyanobacterial populations controlled by physical processes. Journal of Plankton Research 27:61–70.

Carey, C. C., K. L. Cottingham, K. C. Weathers, J. A. Brentrup, N. M. Ruppertsberger, H. Ewing, and N. G. Hairston. 2014. Experimental blooms of the cyanobacterium Gloeotrichia echinulata increase phytoplankton biomass, richness and diversity in an oligotrophic lake. Journal of Plankton Research 36:364–377.

Cottingham, K. L., H. A. Ewing, M. L. Greer, C. C. Carey, and K. C. Weathers. 2015. Cyanobacteria as biological drivers of lake nitrogen and phosphorus cycling. Ecosphere 6:1–19.

Cyr, H. 2017. Winds and the distribution of nearshore phytoplankton in a stratified lake. Water Research 122:114–127.

Dietze, M. C. 2017. Prediction in ecology: A first-principles framework: A. Ecological Applications 27:2048–2060.

Diniz-Filho, A. F., L. M. Bini, T. F. Rangel, R. D. Loyola, C. Hof, D. Nogue, and M. B. Arau. 2009. Partitioning and mapping uncertainties in ensembles of forecasts of species turnover under climate change. Ecography 32:897–906.

Fox, A. M., T. J. Hoar, J. L. Anderson, A. F. Arellano, W. K. Smith, M. E. Litvak, N. MacBean, D. S. Schimel, and D. J. P. Moore. 2018. Evaluation of a Data Assimilation System for Land Surface Models Using CLM4.5. Journal of Advances in Modeling Earth Systems 10:2471–2494.

Gauthier, G., G. Peron, J.-D. Lebreton, P. Grenier, and L. van Oudanhove. 2016. Partitioning prediction uncertainty in climate-dependent population models. Proceedings of the Royal Society B 283:20162353.

Gertner, G., P. Parysow, and B. Guan. 1996. Projection Variance Partitioning of a Conceptual Forest Growth Model with Orthogonal Polynomials. Forest Science 42:474–486.

Huang, J., J. Gao, J. Liu, and Y. Zhang. 2013. State and parameter update of a hydrodynamic-phytoplankton model using ensemble Kalman filter. Ecological Modelling 263:81–91.

Idso, S. B. 1973. On the concept of lake stability. Limnol. Oceanogr. 18:681–683.

Istvánovics, V., K. Pettersson, M. A. Rodrigo, D. Pierson, J. Padiśk, and W. Colom. 1993. Gloeotrichia echinulata, a colonial cyanobacterium with a unique phosphorus uptake and life strategy. Journal of Plankton Research 15:531–552.

Jiang, J., Y. Huang, S. Ma, M. Stacy, Z. Shi, D. M. Ricciuto, P. J. Hanson, and Y. Luo. 2018. Forecasting Responses of a Northern Peatland Carbon Cycle to Elevated CO2 and a Gradient of Experimental Warming. Journal of Geophysical Research: Biogeosciences 123:1057–1071.

Jiang, Y., Q. Zhuang, S. Schaphoff, S. Sitch, A. Sokolov, D. Kicklighter, and J. Melillo. 2012. Uncertainty analysis of vegetation distribution in the northern high latitudes during the 21st century with a dynamic vegetation model. Ecology and Evolution 2:593–614.

Johansson, M. A., K. M. Apfeldorf, S. Dobson, J. Devita, A. L. Buczak, B. Baugher, L. J. Moniz, T. Bagley, S. M. Babin, E. Guven, T. K. Yamana, J. Shaman, T. Moschou, N. Lothian, A. Lane, G. Osborne, G. Jiang, L. C. Brooks, D. C. Farrow, S. Hyun, R. J. Tibshirani, R. Rosenfeld, J. Lessler, N. G. Reich, D. A. T. Cummings, S. A. Lauer, S. M. Moore, H. E. Clapham, R. Lowe, T. C. Bailey, M. García-Díez, M. S. Carvalho, X. Rodó, T. Sardar, R. Paul, E. L. Ray, K. Sakrejda, A. C. Brown, X. Meng, O. Osoba, R. Vardavas, D. Manheim, M. Moore, D. M. Rao, T. C. Porco, S. Ackley, F. Liu, L. Worden, M. Convertino, Y. Liu, A. Reddy, E. Ortiz, J. Rivero, H. Brito, A. Juarrero, L. R. Johnson, R. B. Gramacy, J. M. Cohen, E. A. Mordecai, C. C. Murdock, J. R. Rohr, S. J. Ryan, A. M. Stewart-Ibarra, D. P. Weikel, A. Jutla, R. Khan, M. Poultney, R. R. Colwell, B. Rivera-García, C. M. Barker, J. E. Bell, M. Biggerstaff, D. Swerdlow, L. Mier-Y-Teran-Romero, B. M. Forshey, J. Trtanj, J. Asher, M. Clay, H. S. Margolis, A. M. Hebbeler, D. George, and J. P. Chretien. 2019. An open challenge to advance probabilistic forecasting for dengue epidemics. Proceedings of the National Academy of Sciences of the United States of America 116:24268–24274.

Karlsson-Elfgren, I., P. Hyenstrand, and E. Riydin. 2005. Pelagic growth and colony division of Gloeotrichia echinulata in Lake Erken. Journal of Plankton Research 27:145–151.

Karlsson-Elfgren, I., K. Rengefors, and S. Gustafsson. 2004. Factors regulating recruitment from the sediment to the water column in the bloom-forming cyanobacterium Gloeotrichia echinulata. Freshwater Biology 49:265–273.

Kim, K., M. Park, J. H. Min, I. Ryu, M. R. Kang, and L. J. Park. 2014. Simulation of algal bloom dynamics in a river with the ensemble Kalman filter. Journal of Hydrology 519:2810–2821.

Madgwick, G., I. D. Jones, S. J. Thackeray, J. A. Elliott, and H. J. Miller. 2006. Phytoplankton communities and antecedent conditions:high resolution sampling in Esthwaite Water. Freshwater Biology 51:1798–1810.

Massoud, E. C., J. Huisman, E. Beninca, M. C. Dietze, W. Bouten, and J. A. Vrugt. 2018. Probing the limits of predictability : data assimilation of chaotic dynamics in complex food webs. Ecology Letters 21:93–103.

Mbogga, M. S., X. Wang, and A. Hamann. 2010. Bioclimate envelope model predictions for natural resource management : dealing with uncertainty. Journal of Applied Ecology 47:731–740.

McMaster, G. S., and W. W. W. Wilhelm. 1997. Growing degree-days: one equation, two interpretations. Agricultural and Forest Meteorology 87:291–300.

Ouellet-Proulx, S., O. Chimi Chiadjeu, M. A. Boucher, and A. St-Hilaire. 2017. Assimilation of water temperature and discharge data for ensemble water temperature forecasting. Journal of Hydrology 554:342–359.

Page, T., P. J. Smith, K. J. Beven, I. D. Jones, J. A. Elliott, S. C. Maberly, E. B. Mackay, M. De Ville, and H. Feuchtmayr. 2017. Constraining uncertainty and process-representation in an algal community lake model using high frequency in-lake observations. Ecological Modelling 357:1–13.

Raiho, A., M. Dietze, A. Dawson, C. Rollinson, J. Tipton, and J. McLachlan. 2020. Determinants of Predictability in Multi-decadal Forest Community and Carbon Dynamics. In prep for Global Change Biology.

Spadavecchia, L., M. Williams, and B. E. Law. 2011. Uncertainty in predictions of forest carbon dynamics: Separating driver error from model error. Ecological Applications 21:1506–1522.

Thomas, R. Q., R. J. Figueiredo, V. Daneshmand, B. J. Bookout, L. K. Puckett, and C. C. Carey. 2020. A near-term iterative forecasting system successfully predicts reservoir hydrodynamics and partitions uncertainty. bioRxiv. https://doi.org/10.1101/2020.01.22.915538.

Thomas, R. Q., A. L. Jersild, E. B. Brooks, V. A. Thomas, and R. H. Wynne. 2018. A mid-century ecological forecast with partitioned uncertainty predicts increases in loblolly pine forest productivity. Ecological Applications 28:1503–1519.

Thuiller, W., M. Guéguen, J. Renaud, D. N. Karger, and N. E. Zimmermann. 2019. Uncertainty in ensembles of global biodiversity scenarios. Nature Communications 10:1–9.

Valle, D., C. L. Staudhammer, W. P. Cropper, and P. R. Van Gardingen. 2009. The importance of multimodel projections to assess uncertainty in projections from simulation models. Ecological Applications 19:1680–1692.

Wang, G., T. Oyana, M. Zhang, S. Adu-prah, S. Zeng, H. Lin, and J. Se. 2009. Forest Ecology and Management Mapping and spatial uncertainty analysis of forest vegetation carbon by combining national forest inventory data and satellite images. Forest Ecology and Management 258:1275–1283.

Watling, J. I., L. A. Brandt, D. N. Bucklin, I. Fujisaki, F. J. Mazzotti, S. S. Roma, and C. Speroterra. 2015. Performance metrics and variance partitioning reveal sources of uncertainty in species distribution models. Ecological Modelling 309–310:48–59.

Winslow, L., J. Read, R. Woolway, J. Brentrup, T. Leach, J. Zwart, S. Albers, and D. Collinge. 2019. rLakeAnalyzer: Lake Physics Tools. https://cran.r-project.org/package=rLakeAnalyzer.

Zhang, Y., Y. Zhao, and L. Feng. 2019. Higher contributions of uncertainty from global climate models than crop models in maize-yield simulations under climate change. Meteorological Applications 26:74–82.